Adsorption (2019) 25:833–842
https://doi.org/10.1007/s10450-019-00086-6

Adsorption characteristics of light gases on basalt rock-based zeolite 4A

Kyung-Jun Hwang[1] · Min Jin Hwang[2] · M. S. Balathanigaimani[3] · Kathy Nwe[1] · Yongjoon Youn[1] · Won-Seok Choi[4] · Hyun-A Kim[5] · Jae Woon Nah[6] · Wang Geun Shim[6]

Received: 30 November 2018 / Revised: 9 April 2019 / Accepted: 12 April 2019 / Published online: 16 April 2019
© Springer Science+Business Media, LLC, part of Springer Nature 2019

Abstract
The adsorption characteristics of light gases on basalt rock-based zeolite 4A (BR zeolite-4A) were systematically investigated to evaluate its potential application as an alternative adsorbent for adsorption-based separation processes. We used alkali fusion and hydrothermal procedure to prepare the nanostructured adsorbent, BR zeolite-4A, which was characterized with field emission scanning electron microscopy, X-ray diffraction, and carbon dioxide adsorption apparatus. The single component adsorption equilibrium for CO_2, CH_4, N_2 and H_2 on the BR zeolite-4A was volumetrically determined using a nanoPOROSITY adsorption analyzer at the temperature range from (288.15 to 308.15) K and pressure range from (0.1 to 110) kPa. The experimental results indicate that BR zeolite-4A showed higher adsorption capacities for CO_2 compared to other light gases, indicating the suitable porous material for selective separation by adsorption. Three different isotherm equations, Langmuir, Toth, and Sips, were used to correlate the adsorption isotherm data and the most reasonable results obtained from the Sips model irrespective of the adsorption isotherm types. Isosteric heat of adsorption and adsorption energy distribution function values were calculated and used to further examine the surface energetic heterogeneity of BR zeolite-4A. The pure component adsorption isotherm results were also used to predict the adsorption selectivity for CO_2/N_2, CO_2/CH_4, CO_2/H_2, and CH_4/H_2 binary mixtures (50:50) at different pressure ranges using ideal adsorbed solution theory.

Keywords Adsorption · Basalt rock zeolite · Heterogeneity · IAST · Selectivity

1 Introduction

The adsorption of contaminants on adsorbents is constantly explored because it is applicable to the recovery and removal of contaminants from gas mixtures. A recent study shows that one billion tons of greenhouse gas is released into the atmosphere every year, which causes various problems in human life (Raupach et al. 2007). Many countries that have joined the Kyoto Protocol around the world are continuing to reduce the emissions of greenhouse gas in an attempt to avoid economic penalties (Yu et al. 2008). Mankind is also trying to get green energy sources from biogas instead of fossil fuels to prevent global warming (Pevida et al. 2009).

The biogas is mainly composed of methane (CH_4), and carbon dioxide (CO_2), whereas nitrogen (N_2), and hydrogen

This article belongs to S.I. ISSHAC10, but it reach the press at the time the special issue was published.

Kyung-Jun Hwang and Min Jin Hwang have contributed equally to this work.

✉ Wang Geun Shim
wgshim@sunchon.ac.kr

[1] NanoSD Inc, 11575 Sorrento Valley Rd, San Diego, CA 92121, USA

[2] Department of Environmental System Engineering, Chonnam National University, Yeosu-si, Jeollanam-do 59626, Republic of Korea

[3] Department of Chemical Engineering, Rajiv Gandhi Institute of Petroleum Technology, Jais, Uttar Pradesh 229304, India

[4] Plasma Application R&D Division, Cheorwon Plasma Research Institute, Cheorwon-gun, Gangwon-do 24047, Republic of Korea

[5] Reliability Center, Korea Conformity Laboratories, Yuseong-gu, Daejeon 34027, Republic of Korea

[6] Department of Polymer Science and Engineering, Sunchon National University, Suncheon-si, Jeollanam-do 57922, Republic of Korea

(H_2) are in trace quantities. Therefore, the energy content per unit volume can be increased by removing the impurities from the biogas and increasing the purity of methane (Ranalli 2007). Among the methods of obtaining CH_4, biological anaerobic digestion process can reduce organic wastes and recover useful methane as an energy source (Holm-Nielsen et al. 2009). The gas generated here is called biogas, and CH_4 contained in the biogas can be used as an alternative energy source for natural gas and power generation using boiler fuel, internal combustion engine or gas turbine (Hullu et al. 2008). Apart from biogas, the landfill gas also a good source of methane and it contains 40–60% CH_4, 20–30% CO_2, and other trace gases (Daniel and Dilip 1990). The landfill gas with high CH_4 content can be a useful resource such as natural gas, if the separation of CO_2 from the same can be done more techno-economically.

A commercial technique for separating CO_2 and other impurities in biogas is the absorption method using amine, but it consumes high energy and also the utility section of CO_2 absorption plant is prone to corrosion problem (Zhao et al. 2017). Therefore, the adsorption separation method is considered to be an alternative method for improving the purity of CH_4 in the biogas due to low maintenance cost, easy operation and low energy (Tagliabue et al. 2009). In the case of the adsorption process, pressure swing adsorption (PSA) method is considered as a useful method for CH_4 separation from biogas (Grande 2012). The PSA is a process of separating by using the difference in the amount of adsorbed gas in the adsorbent, and it is easy to operate with small energy consumption.

In the case of adsorbents that can be used for the PSA process, there are activated carbon adsorbents and porous ceramic adsorbents. In recent years, ceramics adsorbents with uniform pores have been developed to be easy to desorb after adsorption and to not decrease adsorption properties even during long-term use (Wang et al. 2011). In particular, adsorbents such as metal-organic framework (MOF) show a very high CO_2 adsorption capacity for high purity of CH_4, but it is difficult to commercialize it as the present technology (Li et al. 2009; Sumida et al. 2012). Porous ceramic adsorbents nowadays have been also developed using natural resources. These materials can be fabricated through the regeneration of existing resources, thus making it possible to easily control the pore-size in the synthetic process with high price competitiveness (Choi et al. 2009).

In our recent report, we demonstrated that basalt rock-based zeolite has a high adsorption affinity for CO_2 at high pressure compared to commercial zeolite (Hwang et al. 2018). The main objective of the present work is thus to examine the potential of the basalt rock-based zeolite for the adsorption separation of other light gases by adsorption (i.e., CH_4, N_2, and H_2) including CO_2 and to extend our previous works to understand the surface heterogeneity and selectivity of the adsorbent. For this purpose, a zeolite 4A prepared from basalt rocks containing a large amount of silicon and aluminum, which is abundantly available in South Korea, is employed as a biogas separation material. The heterogeneous adsorption behaviors of CH_4, CO_2, N_2, and H_2 on basalt-based zeolite 4A have been intensively investigated. In addition, the ideal adsorbed solution theory (IAST), developed by Myers and Prausnitz (1965), was employed to study the adsorption selectivities of prepared zeolite 4A for CO_2/N_2, CO_2/CH_4, CO_2/H_2, and CH_4/H_2 binary mixture using pure component adsorption isotherm experimental results.

2 Experimental

2.1 Preparation

The synthesis of the basalt rock-based zeolite 4A (BR zeolite 4A) was prepared using basalt rock pieces collected from Hantan riverside in Cheorwon-gun, South Korea. The basalt rock pieces were ground into micro-powder using disk mill (Pulverisette 13, Fritsch Co.) and planetary ball mill (Pulverisette 5, Fritsch Co.). The synthetic process of BR zeolite 4A consisted of two steps: (1) alkaline fusion process of micronized BR powder with sodium hydroxide (NaOH, Aldrich Co.) and (2) hydrothermal treatment. First, 20 g of micronized basalt powder and NaOH (1:1.2 g/g ratio) were heated in presence air for alkali-fusion at 1073.15 K for 1 h. The alkalized product was transferred to a 500 ml beaker containing 100 ml of distilled water, which was eluted at room temperature for 2 h after that the extract was collected for further processing. The extracted solution was then separated into a supernatant using 0.4 um PTFE membrane filter. To synthesize the basalt-based zeolite 4A (BR zeolite 4A), 100 ml of the amorphous aluminosilicate extract was taken along with 5 g of sodium aluminum oxide ($NaAlO_2$, Aldrich Co.) in a 500 ml round flask. The entire mixture and stirred at 250 rpm under reflux conditions and finally the hydrothermal treatment was carried out at 363.15 K for 12 h. At the end, the crystallized solid part was separated, washed and followed by overnight drying at 373.15 K.

2.2 Adsorbent characterization and adsorption measurements

The synthesized materials were characterized using X-ray diffraction (XRD), Field emission scanning microscopy (FE-SEM, S-4700, Hitachi Co.), and energy dispersive X-ray spectroscopy (EDX) techniques. The XRD patterns were obtained from a D/MAX-2500 (Rigaku Co.) unit with Cu–Kα radiation ($\lambda = 1.540$ Å) and interpreted with the help of the XRD database of the International Zeolite Association (IZA) (Treacy et al. 2001). The crystallite size was

calculated from the XRD results applying Scherrer equation (Holzwarth and Gibson 2011). The textural characteristics of prepared BR zeolite 4A were determined from CO_2 adsorption isotherm data measured at 298.15 K in a nanoPorosity-XG apparatus (MiraeSI Co.). It may be noted here that we already demonstrated in our previous work that CO_2 would be a suitable probe molecule to characterize the super microporous adsorbent compared to N_2 due to its kinetic effects (Breck 1974; Hwang et al. 2018; Jensen et al. 2012). The BET surface area and Dubinin–Radushkevich (DR) pore volume of BR zeolite 4A were 726 m^2/g and 0.345 cm^3/g, respectively.

The single component adsorption isotherms of CO_2, CH_4, N_2 and H_2 on BR zeolite 4A were measured volumetrically with the nanoPorosity-XG apparatus (MiraeSI Co.) at different temperatures of (288.15, 298.15, and 308.15) K with the gas pressure up to 110 kPa, respectively. Before the adsorption measurements, about 100 mg of adsorbent was loaded into an adsorption cell and the sample was then evacuated at 773.15 K under vacuum for 24 h to remove the moisture and trace pollutants presented in the adsorbent. Moreover, the desorbed samples were also regenerated at 773.15 K under vacuum for 24 h before initiation of each experiment. The high purity gases (> 99.99%) were used for adsorption measurements.

3 Results and discussion

We synthesized a BR zeolite 4A with homogeneous pores from the optimum conditions (Hwang et al. 2018) and showed the morphology (FE-SEM images) and crystallinity (XRD peaks) of the same material in Fig. 1. The chemical composition of micronized BR powders and synthesized BR zeolite 4A samples were compared by EDX analysis. The raw BR material is mostly composed of 48.2% oxygen (O), 12.3% aluminum (Al) and 19.9% silicon (Si), with the remainder consisting of 6.2% calcium (Ca), 4.7% magnesium (Mg), 3.2% potassium (K), 3.0% iron (Fe), and 2.6% sodium (Na), respectively. These results are similar to the mineralogical information of basalt rocks as known well in the region of Gangwon province, South Korea (Yoon and Kim 2015). Here, trace minerals such as Ca, Mg, K, and Fe can interrupt the nucleation of Na based aluminosilicate in hydrothermal treatment (Xiao et al. 2015). Therefore, the useless minerals will be removed for the synthesis of high purity BR zeolite 4A. According to the results of EDX analysis, the synthesized BR zeolite 4A was composed of 61.5% O, 13.1% Na, 12.5% Si, and 12.9% Al in the Na/Al/Si ratio of around 1:1:1 (the Na/Al/Si ratio of typical zeolite Na4A is 1:1:1) (Rayalu et al. 1999). Also, no trace impurities of micronized BR powders other than the major components of the zeolite Na4A were observed. We confirmed that all impurities of micronized BR powders were removed through the acidic treatment before the alkali-fusion annealing process.

The surface morphology of raw basalt material used for the synthesis of BR zeolite 4A is shown in Fig. 1a, which shows that the pattern of fine particles with irregular shapes within about 5 μm after disk milling and planetary milling. In general zeolite synthetic process, a fine mineral precursor is easy to perform the alkali-fusion reaction due to the high specific surface area and the elution process for a specific component. The FE-SEM image of BR zeolite 4A is presented in Fig. 1b. The particle size of the BR zeolite 4A is about 1–5 μm, and the particle shape is regular cubic, which matches with the typical shape of Na4A zeolite (Loiola et al. 2012). Figure 1c shows the XRD spectra of BR zeolite 4A

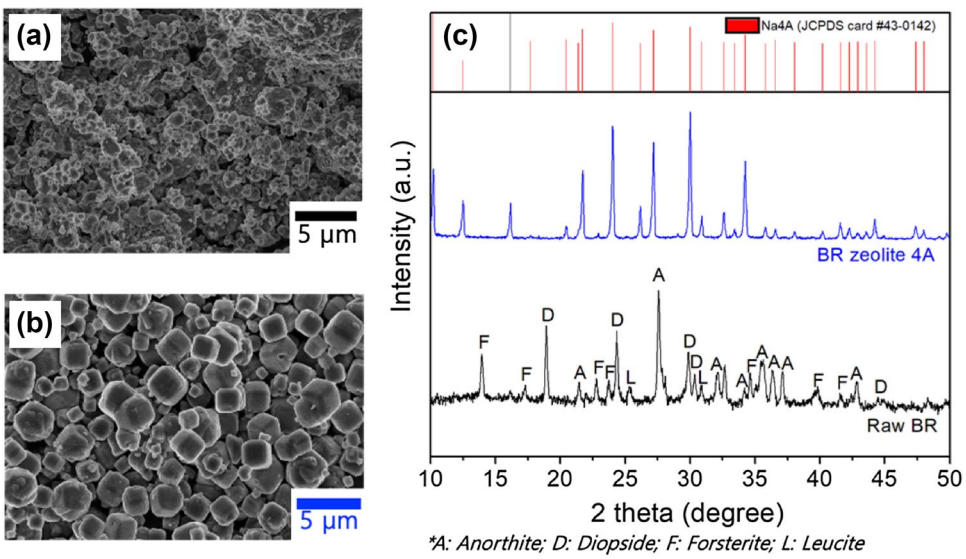

Fig. 1 FE-SEM images (**a** raw BR, **b** BR zeolite 4A) and XRD peaks (**c**) of BR zeolite 4A

before and after hydrothermal synthesis. The crystal structure of the raw BR material before synthesis was 38.7% Anorthite [(Ca,Na)(Al, Si)$_2$Si$_2$O$_8$, JCPDS card #20-0528], 28% Forsterite [(Mg, Fe) $_2$SiO$_4$, JCPDS card #31-0795], 26.1% Diopside [CaMg(SiO$_3$)$_2$, JCPDS card #11-0654], and 7.2% Leucite [K(AlSi$_2$O$_6$), JCPDS card #15-0047], which is consistent with the previous mineralogical information (Yoon and Kim 2015). The XRD peaks of BR zeolite 4A after synthesis were all the same as those of typical zeolite Na4A (JCPDS card #43-0142) (Xiao et al. 2015). Therefore, in the case of BR zeolite 4A, the pore size is estimated to be about 4 Å, and the average crystallite size calculated by the Scherrer equation is 800 nm (Holzwarth and Gibson 2011).

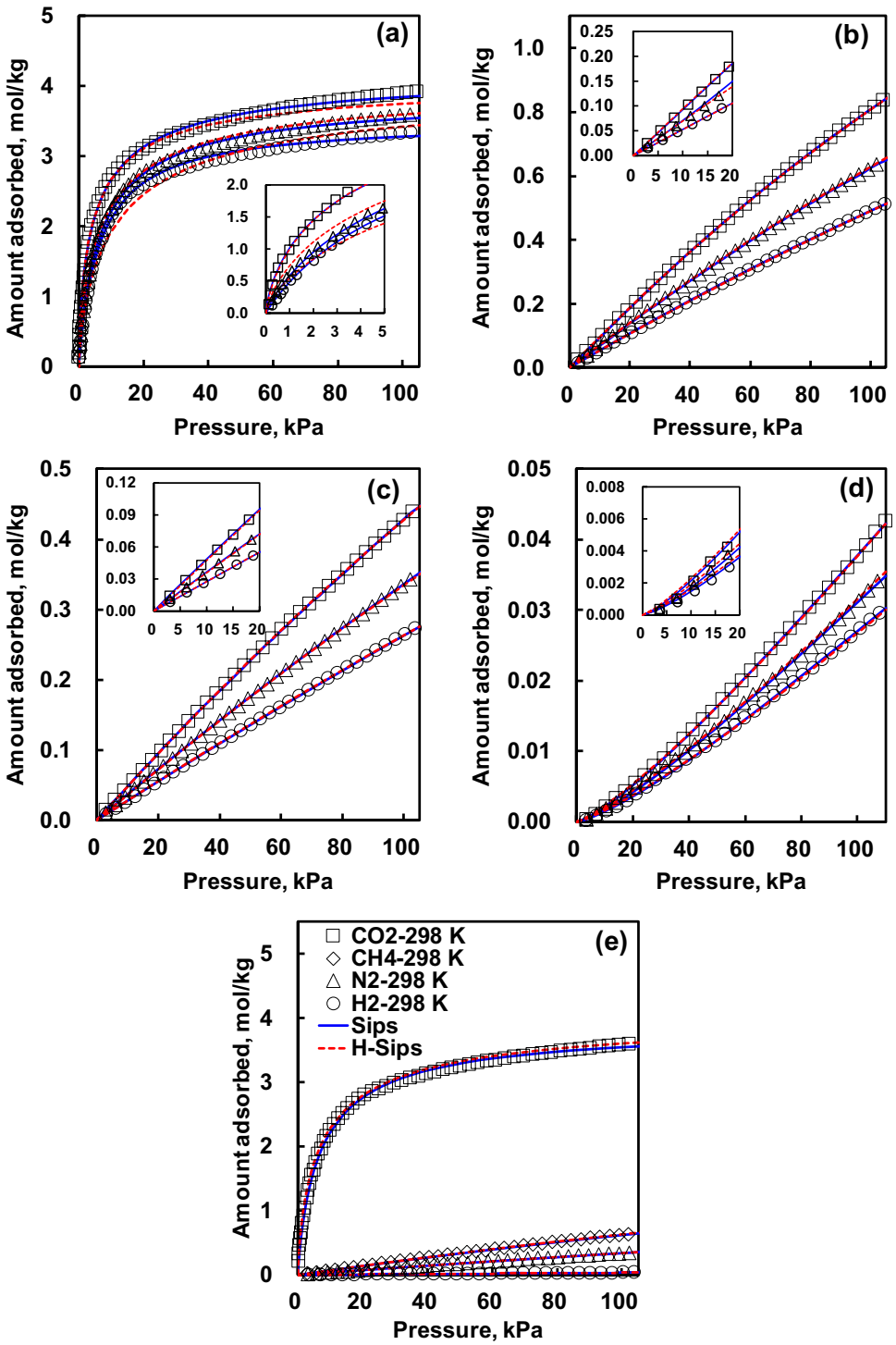

Fig. 2 Adsorption isotherms of **a** CO_2, **b** CH_4, **c** N_2, and **d** H_2 on BR-Zeolite 4A (square, T = 288 K; triangle, T = 298 K; circle, T = 308 K; dark blue line, Sips; dotted red line, temperature-dependent Sips). Comparison of experimental CO_2, CH_4, N_2, and H_2 adsorption isotherms at 298.15 K (Sips, isothermal Sips model; H-Sips, temperature-dependent Sips model) (**e**)

Adsorption equilibrium isotherms of CO_2, N_2, CH_4, and H_2 on BR-Zeolite 4A obtained at three different temperatures (288.15, 298.15, and 308.15) K and at pressure up to 110 kPa are presented in Fig. 2a–d. As shown in this figure, the adsorption amounts of CO_2 were much greater than those of CH_4, N_2, and H_2 in the tested pressure and temperature ranges. In addition, CO_2 adsorption isotherm clearly shows a type I (convex) behavior revealing the high adsorbent–adsorbate interactions in micropores according to the IUPAC classification, but other gas isotherms follow linear or weakly favorable (CH_4 and N_2) and unfavorable (H_2) pattern. The comparative adsorption isotherm plots for the light gases, which is shown in Fig. 2e, clearly indicated that carbon dioxide (3.61 mol/kg) uptake on BR-Zeolite 4A at 298.15 K and 110 kPa is significantly higher than other gases tested: CH_4 (0.63 mol/kg), N_2 (0.34 mol/kg), and H_2 (0.03 mol/kg). The measured adsorption amounts were relatively lower than those of reported values at given experimental conditions (≈4.2 mol/kg for CO_2, ≈0.8 mol/kg for CH_4, ≈1.3 mol/kg for N_2, and ≈0.4 mol/kg for H_2) (Akten et al. 2003; Bacsik et al. 2016). However, the adsorption behavior observed is similar to those of previous reports. This result clearly indicates that the prepared BR-Zeolite 4A is specifically selective for the adsorption of CO_2 over other light gases studied, which shows more evidentially that BR-Zeolite 4A can selectively separate CO_2 from a multicomponent gas mixture system. In addition, it was further observed in this study the adsorption capacity was closely connected with the polarizability of adsorbate rather than quadrupole moment and dipole moment. The polarizability ($\times 10^{-25}$ cm^3) values of the light gases tested in this work are in the following order: CO_2 (29.1) > CH_4 (26.0) > N_2 (17.4) > H_2 (9.11). The above mentioned trend is exactly match with the adsorption patterns of BR-Zeolite 4A, which clearly confirms the role of polarizability in adsorption of gases on BR-Zeolite 4A. Moreover, the adsorption capacities of all gases decrease with increasing temperature, indicating the dominant physisorption interaction between the BR-Zeolite 4A and light gases.

Three well-known isotherm equations, Langmuir, Toth, and Sips with different advantage and limitations were used to correlate each experimental adsorption isotherm data. The model isotherm equations used in this work were summarized in Table 1 (Do 1998; Jaroniec and Madey 1988; Malek and Farooq 1996; Rudzinski and Everett 1991). To assess the goodness of fit of experimental isotherm data, the average relative error (ARE) listed in Table 1 was also used in this work. The Nelder–Mead pattern search algorithm was used to determine the optimum isotherm parameters for each case. Tables 2 and 3 summarize the isotherm and the temperature dependent isotherm parameters with the respective ARE values. As shown in Fig. 2 (the other fitting results are not shown here for simplicity), the Sips and the temperature dependent Sips equations reasonably well correlates all the experimental adsorption isotherm data over the entire pressure and temperature ranges studied. The Sips isotherm parameter n values, which indicate the system heterogeneity, are in the range of 1.029–1.385 for CO_2, 0.961–0.975 for CH_4, 0.993–1.018 for N_2, and 0.769–0.779 for H_2, respectively. In addition, the temperature dependent Sips isotherm parameter n values are 1.315 (CO_2), 0.981 (CH_4), 0.984 (N_2), and 0.816 (H_2), respectively. These results indicate that the degree of heterogeneity of CO_2/BR-Zeolite 4A is the greatest compared to other light gases system measured in this work. It is also interesting to note from Tables 2 and Table 3 that the Toth and the temperature dependent Toth equations give similar or better ARE correlation results than the Sips and the temperature dependent Sips models for CO_2, CH_4, and N_2. Very poor correlation results are, however, obtained for H_2, which are similar to those of the Langmuir and the temperature dependent Langmuir equations. These results indicate that among the isotherm equation, the Sips equation is the most suitable to predict the binary mixture equilibria when incorporating the ideal adsorbed solution theory.

Table 1 List of single component adsorption isotherm equations and average relative error (ARE) equation used in this work

Isotherm	Mathematical form	Parameter
Langmuir	$q = \frac{q_s bP}{1+bP}$ $b = b_0 exp\left(-\frac{\Delta H_A}{RT}\right)$	q_s [mmol/g] b [1/kPa] b_0 [1/kPa] $-\Delta H_A$ [kJ/mol]
Toth	$q = \frac{q_s bP}{(1+(bP)^t)^{1/t}}$ $b = b_0 exp\left(-\frac{\Delta H_A}{RT}\right)$	q_s [mmol/g] b [1/kPa] b_0 [1/kPa] $-\Delta H_A$ [kJ/mol] t [-]
Sips	$q = \frac{q_s bP^{1/n}}{1+bP^{1/n}}$ $b = b_0 exp\left(-\frac{\Delta H_A}{RT}\right)$	q_s [mmol/g] b [1/kPa] b_0 [1/kPa] $-\Delta H_A$ [kJ/mol] n [-]
Error	$ARE(\%) = \frac{100}{N}\sum_{i=1}^{N}\frac{\lvert q_{exp}-q_{cal}\rvert}{q_{exp}}$	

In order to further investigate the interactions existing between the adsorbent and adsorbate as well as between the adsorbate and adsorbate in the adsorbed phase, the isosteric heat of adsorption was calculated from the pure component adsorption isotherm data using the Clausius–Claypeyon equation (Do 1998; Jaroniec and Madey 1988; Rudzinski and Everett 1991). This equation has the following form:

$$\frac{q_{st}}{RT^2} = \left[\frac{\partial lnP}{\partial T}\right]_q \quad (1)$$

where q_{st}, P, T, and R are the isosteric heat of adsorption, the gas constant, temperature, and pressure, respectively.

Table 2 Isotherm parameters of Langmuir, Toth, and Sips models for CO_2, CH_4, N_2, and H_2 on BR zeolite 4A

Model	Parameters	CO_2			CH_4			N_2			H_2		
		288	298	308	288	298	308	288	298	308	288	298	308
Langmuir[a]	q_s [mmol/g]	3.995	3.621	3.428	4.727	4.688	4.649	4.633	3.796	3.428	5.055	4.278	3.407
	b [1/kPa]	0.206	0.184	0.170	0.0021	0.0015	0.0012	1.02E−3	9.72E−4	8.30E−4	7.61E−5	7.21E–5	7.01E–5
	ARE	8.578	4.233	3.313	0.939	0.776	0.476	1.085	0.113	0.724	34.530	32.663	47.195
Toth[b]	q_s [mmol/g]	4.511	4.299	3.708	2.399	2.185	2.004	3.850	3.607	3.375	0.168	0.743	0.282
	b [1/kPa]	0.582	0.256	0.233	0.0039	0.0032	0.0027	1.27E–3	1.02E–3	8.26E–4	2.16E–3	3.99E–4	9.14E–4
	t [-]	0.581	0.645	0.754	1.466	1.483	1.491	0.956	1.019	1.109	24.562	9.952	11.459
	ARE	3.681	4.449	3.019	0.350	0.281	0.269	0.126	0.106	0.085	34.134	31.827	46.710
Sips[c]	q_s [mmol/g]	4.291	3.900	3.510	3.580	3.567	3.488	4.385	4.147	3.909	0.457	0.371	0.318
	b [1/kPa]	0.310	0.176	0.160	0.0024	0.0018	0.0014	1.18E–3	9.02E–4	7.01E–4	2.45E–4	2.39E–4	2.33E–4
	n [-]	1.385	1.145	1.029	0.961	0.969	0.975	1.018	1.005	0.993	0.779	0.774	0.769
	ARE	4.743	3.030	3.900	0.087	0.113	0.185	0.471	0.206	0.162	6.759	7.314	12.885

[a]Langmuir: $q = \frac{q_s bP}{1+bP}$

[b]Toth: $q = \frac{q_s bP}{\left(1+(bP)^t\right)^{1/t}}$

[c]Sips: $q = \frac{q_s bP^{1/n}}{1+bP^{1/n}}$

Table 3 Temperature dependent isotherm parameters of Langmuir, Toth, and Sips models for CO_2, CH_4, N_2, and H_2 on BR zeolite 4A

Model	Parameters	CO_2	CH_4	N_2	H_2
Langmuir[a]	q_s[mmol/g]	3.721	4.674	3.565	0.634
	b_0 [1/kPa]	1.212E–7	2.578E–7	3.531E–7	9.521E–6
	$-\Delta H_A$ [kJ/mol]	3.518E+4	2.157E+4	1.979E+4	9.816E+3
	ARE	6.053	0.821	0.440	41.990
Toth[b]	q_s [mmol/g]	4.308	3.231	1.908	0.103
	b_0 [1/kPa]	1.892E–7	3.605E–7	6.363E–7	1.777E–5
	$-\Delta H_A$ [kJ/mol]	3.559E+4	2.160E+4	1.983E+4	1.266E+4
	t [-]	0.620	1.203	1.327	5.745
	ARE	3.774	0.663	0.370	37.650
Sips[c]	q_s [mmol/g]	4.097	4.019	2.971	1.763
	b_0 [1/kPa]	3.415E–6	2.342E–7	3.491E–7	3.658E–7
	$-\Delta H_A$ [kJ/mol]	2.744E+4	2.203E+4	2.014E+4	1.2818E+4
	n [-]	1.315	0.981	0.984	0.816
	ARE	3.788	0.559	0.381	11.418

[a]Langmuir: $q = \frac{q_s b_0 exp\left(-\frac{\Delta H_A}{RT}\right)P}{1+b_0 exp\left(-\frac{\Delta H_A}{RT}\right)P}$

[b]Toth: $q = \frac{q_s b_0 exp\left(-\frac{\Delta H_A}{RT}\right)P}{\left(1+\left(b_0 exp\left(-\frac{\Delta H_A}{RT}\right)P\right)^t\right)^{1/t}}$

[c]Sips: $q = \frac{q_s b_0 exp\left(-\frac{H_A}{RT}\right)P^{1/n}}{1+b_0 exp\left(-\frac{\Delta H_A}{RT}\right)P^{1/n}}$

Figure 3a compares the variation of isosteric heat of adsorption along with the adsorbed amount for CO_2, N_2, CH_4, and H_2 on BR-Zeolite 4A. The experimental adsorption data were fitted with polynomial regression functions to properly represent the isosteric heat curves. As shown in this figure, the degree of variation trends for the isosteric heat of adsorption is greatly dependent on the probe molecules used, revealing the existence of different interactions in the adsorption system closely related with the energetical and structural heterogeneity of the porous materials. The overall magnitudes of the average isosteric heat of adsorption are in the following decreasing order: CO_2 (36.2 kJ mol^{-1}) > CH_4

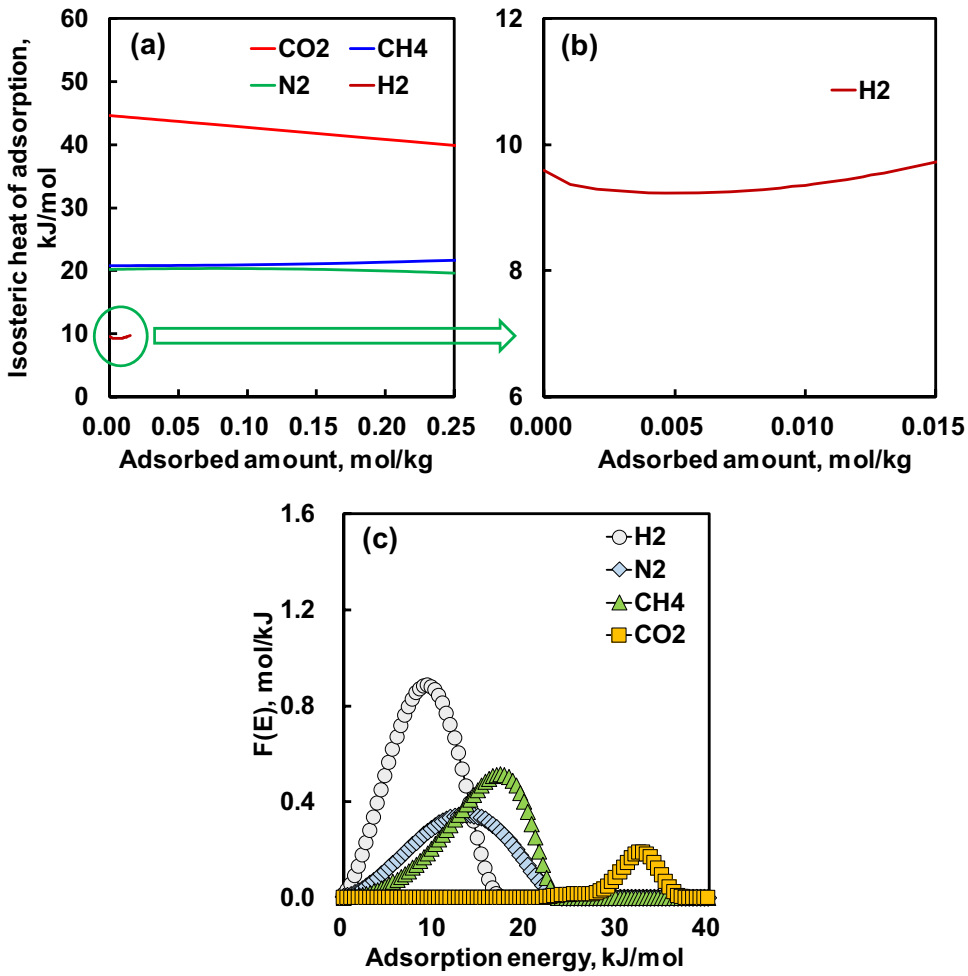

Fig. 3 Isosteric heat of adsorption (**a**, **b**) and adsorption energy distribution curves (**c**) of CO_2, CH_4, N_2, and H_2 on BR zeolite 4A

(21.8 kJ mol^{-1}) > = N_2 (20.5 kJ mol^{-1}) > H_2 (10.4 kJ mol^{-1}). These calculated isosteric heat of adsorption were in a similar ranges as in previous reports (≈28–35 kJ mol^{-1} for CO_2, ≈18.8 kJ mol^{-1} for CH_4, ≈17 kJ mol^{-1} for N_2, and ≈10 kJ mol^{-1} for H_2) (Akten et al. 2003; Grande and Blom 2014). It is also interesting to note that the curves can be classified into three groups. As shown in this figure, the isosteric heat curves for light gases adsorption show meaningful dependence on the adsorbed amount within in our experimental range. The isosteric heat curves for CO_2 continuously decrease with increasing adsorbed amounts, suggesting the relatively strong dominance of vertical (adsorbate–adsorbent) interaction related with the existence of surface energetic heterogeneity of BR-Zeolite 4A/CO_2 adsorption system.

On the other hand, the isosteric heat trends of CH_4 and N_2 are very similar within the experimental range, indicating the similar adsorption affinity behavior. These isosteric heat curves slightly increase with increasing adsorbed amount, revealing the relative importance of the lateral (CH_4–CH_4 and N_2–N_2) interactions compare to that of the vertical [CH_4 (or N_2)–BR-Zeolite 4A] interactions in the CH_4 and N_2 adsorption system. In addition, the isosteric heat trend of H_2 is slightly different from those of CO_2, N_2, and CH_4. As shown in Fig. 3b, the H_2 isosteric heat curve can be classified into three parts: (1) initially decrease with the increasing adsorbed amount, (2) approaching the minimum value, and (3) then again slightly increase with the increasing adsorbed amount. This result clearly indicates that in this case the H_2–BR-Zeolite 4A surface interaction initially controls the system and its interaction gradually decreases with increasing H_2 adsorption. Then H_2–H_2 lateral interaction dominates the adsorption system as the H_2 adsorption increases.

The adsorption energy distribution (AED) function is also useful to understand the surface energetic heterogeneity of porous materials (Do 1998; Hwang et al. 2015; Jaroniec and Madey 1988; Nahm et al. 2012; Rudzinski and Everett 1991).

$$\theta(p) = \int_{\Delta} \theta(p, E) F(E) dE \tag{2}$$

where p, E, Δ, θ(p), θ(p, E), and F(E) are the pressure, the adsorption energy, the integration region, the experimental adsorption isotherm data, a local adsorption isotherm with

an adsorption energy, and the adsorption energy distribution function, respectively.

In this work, the Langmuir adsorption equation and the generalized nonlinear regularization method were used to calculate the adsorption energy distribution function for all gases. Figure 3c compares the AED curves of four gases on BR-Zeolite 4A. The peak shape of calculated AED is greatly dependent on the molecules used. All adsorbates represent single peak with different peak width, peak height, and peak maximum, indicating the existence of one predominant type of surface energetic heterogeneity for BR-Zeolite 4A. The peak maximum appeared at about 32.8 (CO_2), 17.2 (CH_4), 13.4(N_2), and 9.2 (H_2) kJ/mol, respectively. These determined values are in the similar ranges of values calculated from the isosteric heat of adsorption. They also have the same order of the magnitudes of the average isosteric heat of adsorption, which is in good agreement with the magnitude order of polarizability tested in this work.

It is clear from pure component adsorption data that the BR zeolite 4A represents preferential adsorption behavior of CO_2 compare to those of other light gases (CH_4, N_2, and H_2). To properly examine the gas separation and purification performance efficiency of the BR zeolite 4A, the adsorption equilibrium selectivity was calculated using the ideal adsorbed solution theory (IAST) which was first proposed by Myers and Prausnitz (1965). In this work, CO_2/N_2, CO_2/CH_4, CO_2/H_2, and CH_4/H_2 binary mixtures at 298.15 K for equimolar condition (50%/50%) were chosen for the comparison study. The Sips isotherm equation was used to predict the binary mixture adsorption equilibria because this equation is more suitable to fit the single component experimental isotherm data compare to other isotherm models as already discussed in the previous section (see Fig. 2 and Tables 2 and 3). The IAST-adsorption equilibrium selectivity, S_{12}, for binary gas mixture can be generally written in the following form:

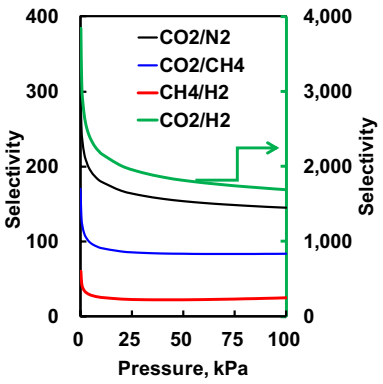

Fig. 4 Adsorption selectivity of binary mixtures CO_2/N_2, CO_2/CH_4, CO_2/H_2, and CH_4/H_2 on BR zeolite 4A

$$S_{12} = \frac{x_1/y_1}{x_2/y_2} \tag{3}$$

where x_1 and x_2 are the mole fraction of component 1 and 2 in the adsorbed phase, y_1 and y_2 are the mole fraction of component 1 and 2 in the gas phase. Figure 4 compares CO_2/N_2, CO_2/CH_4, CO_2/H_2, and CH_4/H_2 selectivities as a function of total pressure for BR zeolite 4A calculated at 298.15 K. On the whole, the IAST-adsorption equilibrium selectivity for all tested cases sharply decreases with increasing total pressure in the low-pressure region followed by no meaningful change as continuously increasing the total pressure which can be closely connected with the interaction between adsorbate and adsorbent. The order of average IAST-calculated adsorption selectivity for binary mixtures at given pressure range was CO_2/H_2 (2246) $\gg$ CO_2/N_2 (186) > CO_2/CH_4 (98) > CH_4/H_2 (28). The average CO_2/H_2 adsorption selectivity is higher than CO_2/N_2 (12 times) and CO_2/CH_4 (23 times) selectivities, which once again prove and confirm the effects of polarizabilities of individual gases on adsorption as well as selectivity, as discussed in the single component isotherm section. In the case of CO_2 over H_2, N_2, and CH_4 selectivity, the greater the difference in polarizability between adsorbates, the higher the adsorption selectivity is. It is also interesting to observe that in case of CH_4 related IAST adsorption selectivity, no evident pattern was observed between the adsorption selectivity and the polarizability. The polarizability of CH_4 is higher than that of H_2 but similar to that of CO_2. The quadrupole moment ($\times 10^{-26}$ esu *cm*) values of tested gases are in the following descending order; CO_2 (4.30) > N_2 (1.52) > H_2 (0.52) > CH_4 (0). In the case of IAST CO_2/CH_4 and CH_4/H_2 selectivities, the greater the difference in quadrupole moment between adsorbates, the higher the adsorption selectivity is.

The calculated IAST adsorption selectivities of BR zeolite 4A were also compared to other zeolite materials to further evaluate the degree of selectivity performance for light gases. As discussed above, in our calculation, the IAST-calculated average CO_2/H_2 selectivity (2246) is the highest examined cases, which was significantly high compared to that of zeolite NaA case (selectivity ratio about 70 at 1 bar for 1.4:98.6) (Belmabkhout and Sayari 2009). Moreover, the IAST-calculated average CO_2/N_2 selectivity (186) is much larger than those of other zeolites under similar measured conditions, which were in the range of about 7.6–8.4 (ZIF-8), 6.9–57.0 (clinoptilolite and cation exchanged clinoptilolites), 44–54 (T-type zeolite), and 45–54 (cation exchanged zeolite), respectively, (Cheung and Hedin 2014; Jiang et al. 2013; Kennedy and Tezel 2018; McEwen et al. 2013) but comparable to those of zeolite 5A and zeolite 13X, which was about 241 and about 190, respectively. (McEwen et al. 2013; Saha et al. 2010) In addition, the IAST-calculated

average selectivity value for CO_2/CH_4 (98) is about 2.6 times lower than that of zeolite 5A (Saha et al. 2010) but is about 1.3(zeolite-NaX), 2.3(zeolite-CaA), 2.7(zeolite-NaA), 4.6(zeolite-CaX), 6 (zeolite 13X and T-type zeolite), 15(zeolite 4A), 20(zeolite-Y and ZSM-5), 25(chabazite), 26(H^+ modernite), 36 (ZIF-8), 1.3–32 (clinoptilolite and cation exchanged clinoptilolites), and 18–28 (high silica zeolites) times greater than those of commercial and natural zeolites under similar conditions (Belmabkhout and Sayari 2009; Jensen et al. 2012; Jiang et al. 2013; Kennedy and Tezel 2018; Li et al. 2013; McEwen et al. 2013). These comparison results indicate that BR zeolite 4A has a great potential application for gas separation by adsorption processes.

4 Conclusion

The BR zeolite 4A, which was prepared from basalt rock by applying alkali fusion and the hydrothermal procedures, was used to investigate the adsorption of CO_2, CH_4, N_2 and H_2 at three different temperatures (288.15, 298.15, and 308.15) K and pressure up to 110 kPa. Our experimental results clearly show that the BR zeolite 4A could be a good potential candidate for light gas separation by adsorption because of its high adsorption affinity and selectivity to CO_2. The order of adsorption capacity was $CO_2 \gg CH_4, > N_2 > H_2$, which indicates that the BR zeolite 4A is the most suitable for CO_2 separation compared to other gases and is also not the desirable one for H_2 adsorption. In addition, the adsorption order of individual light gases on BR zeolite 4A is also identical with their polarizability values. The Sips isotherm model fit well the single component experimental data for all gases over the experimental ranges compared to Langmuir and Toth isotherm models. The results of isosteric heat of adsorption and adsorption energy distribution of CO_2, CH_4, N_2 and H_2 on BR zeolite 4A clearly revealed that the surface of BR zeolite 4A is energetically heterogeneous. Moreover, the variation trend of isosteric heat of adsorption and adsorption energy distribution can be well correlated with the polarizability of gases used. The IAST adsorption selectivity performance for CO_2/N_2, CO_2/CH_4, CO_2/H_2, and CH_4/H_2 has a close connection with their pure component adsorption affinity, the polarizability, and the quadrupole moment values. Our results also indicate that calculated average IAST adsorption selectivities of the BR zeolite 4A represented the highest CO_2 selectivity over N_2, CH_4, and H_2, revealing its high competitiveness in selective separation by adsorption.

Acknowledgements This work was supported by the Basic Science Research Program through the National Research Foundation of Korea (NRF) funded by the Ministry of Education (Grant No. NRF-2017R1D1A3B03034385) and the author gratefully acknowledge the financial support from the Ministry of Trade, Industry and Energy (MOTIE) and the Korean Energy Technology Evaluation and Planning (KETEP) (Grant No. 20153030013010).

References

Akten, E.D., Siriwardane, R., Sholl, D.S.: Monte carlo simulation of single-and binary-component adsorption of CO_2, N_2, and H_2 in zeolite Na-4A. Energy Fuel **17**, 977–983 (2003)

Bacsik, Z., Cheung, O., Vasiliev, P., Hedin, N.: Selective separation of CO_2 and CH_4 for biogas upgrading on zeolite NaKA and SAPO-56. Appl. Energy **162**, 613–621 (2016)

Belmabkhout, Y., Sayari, A.: Adsorption of CO_2 from dry gases on MCM-41 silica at ambient temperature and high pressure. 2: adsorption of CO_2/N_2, CO_2/CH_4 and CO_2/H_2 binary mixtures. Chem. Eng. Sci. **64**, 3729–3735 (2009)

Breck, D.W.: Zeolite molecular sieves: structure, chemistry, and use. Wiley, New York (1974)

Cheung, O., Hedin, N.: Zeolites and related sorbents with narrow pores for CO_2 separation from flue gas. RSC Adv. **4**, 14480–14494 (2014)

Choi, S., Drese, J.H., Jones, C.W.: Adsorbent materials for carbon dioxide capture from large anthropogenic point sources. Chemsuschem **2**, 796–854 (2009)

Daniel, A.L., Dilip, R.A.: Relative contributions of greenhouse gas emissions to global warming. Nature **344**, 529–531 (1990)

Do, D.D.: Adsorption analysis: equilibria and kinetics. Imperial College Press, London (1998)

Grande, C.A.: Advances in pressure swing adsorption for gas separation. ISRN Chem. Eng. **2012**, 1–13 (2012)

Grande, G.A., Blom, R.: Cryogenic adsorption of methane and carbon dioxide on zeolites 4A and 13X. Energy Fuel **28**, 6688–6693 (2014)

Holm-Nielsen, J.B., Al, S.T., Oleskowicz-Popiel, P.: The future of anaerobic digestion and biogas utilization. Bioresour. Technol. **100**, 5478–5484 (2009)

Holzwarth, U., Gibson, N.: The Scherrer equation versus the 'Debye-Scherrer equation'. Nat. Nanotech. **6**, 534 (2011)

Hullu, J., Maassen, J.I.W., van Meel, P.A., Shazad, S., Vaessen, J.M.P.: Comparing different biogas upgrading techniques-final report. Eindhoven University of Technology (2008)

Hwang, K.J., Choi, W.S., Jung, S.H., Kwon, Y.J., Hong, S., Choi, C., Lee, J.W., Shim, W.G.: Synthesis of zeolitic material from basalt rock and its adsorption properties for carbon dioxide. RSC Adv. **8**, 9524–9529 (2018)

Hwang, K.J., Park, J.Y., Kim, Y.J., Kim, G., Choi, C., Jin, S., Kim, N., Lee, J.W., Shim, W.G.: Adsorption behavior of dyestuffs on hollow activated carbon fiber from biomass. Sep. Sci. Technol. **50**, 1757–1767 (2015)

Jaroniec, M., Madey, R.: Physical Adsorption on Heterogeneous Solids. Elsevier, Amsterdam (1988)

Jensen, N.K., Rufford, T.E., Watson, G., Zhang, D.K., Chan, K.I., May, E.F.: Screening zeolites for gas separation applications involving methane, nitrogen, and carbon dioxide. J. Chem. Eng. Data **57**, 106–113 (2012)

Jiang, Q., Rentschler, J., Sethia, G., Weinman, S., Perrone, R., Liu, K.: Synthesis of T-type zeolite nanoparticles for the separation of CO_2/N_2 and CO_2/CH_4 by adsorption process. Chem. Eng. J. **230**, 380–388 (2013)

Kennedy, D.A., Tezel, F.H.: Cation exchange modification of clinoptilolite – Screening analysis for potential equilibrium and kinetic adsorption separations involving methane, nitrogen, and carbon dioxide. Microporous Mesoporous Mater. **262**, 235–250 (2018)

Li, J.-R., Kuppler, R.J., Zhou, H.-C.: Selective gas adsorption and separation in metal–organic frameworks. Chem. Soc. Rev. **38**, 1477–1504 (2009)

Li, Y., Yi, H., Tang, X., Li, F., Yuan, Q.: Adsorption separation of CO_2/CH_4 gas mixture on the commercial zeolites at atmospheric pressure. Chem. Eng. J. **229**, 50–56 (2013)

Loiola, A.R., Andrade, J.C.R.A., Sasaki, J.M., da Silva, L.R.D.: Structural analysis of zeolite NaA synthesized by a cost-effective hydrothermal method using kaolin and its use as water softener. J. Colloid Interface Sci. **367**, 34–39 (2012)

Malek, A., Farooq, S.: Comparison of isotherm models for hydrocarbon adsorption on activated carbon. AIChE J. **42**, 3191–3201 (1996)

McEwen, J., Hayman, J.-D., Ozgur, Y.A.: A comparative study of CO_2, CH_4 and N_2 adsorption in ZIF-8, Zeolite-13X and BPL activated carbon. Chem. Phys. **412**, 72–76 (2013)

Myers, A.L., Prausnitz, J.M.: Thermodynamics of mixed gas adsorption. AIChE J. **11**, 121–127 (1965)

Nahm, S.W., Shim, W.G., Park, Y.K., Kim, S.C.: Thermal and chemical regeneration of spent activated carbon and its adsorption property for toluene. Chem. Eng. J. **210**, 500–509 (2012)

Pevida, M.G.C., Arias, B., Casal, M.D., Martín, C.F., Fermoso, J., Rubiera, F., Pis, J.J.: Different approaches for the development of low-cost CO_2 adsorbents. J. Environ. Eng. **135**, 426–432 (2009)

Ranalli, P.: Improvement of crop plants for industrial end uses. Springer, The Netherlands (2007)

Raupach, M.R., Marland, G., Ciais, P., Le Quéré, C., Canadell, J.G., Klepper, G., Field, C.B.: Global and regional drivers of accelerating CO_2 emissions. Proc. Natl. Acad. Sci. U.S.A. **104**, 10288–10293 (2007)

Rayalu, S.S., Meshram, S.U., Hasan, M.Z., Kaul, S.N.: Fly Ash Based Zeolite Technology. In: An illustration of waste to wealth. proceedings of the fifteenth international conference on solid waste technology and management. Philadelphia, USA (1999)

Rudzinski, W., Everett, D.: Adsorption of gases on heterogeneous solid surfaces. Academic Press, London (1991)

Saha, D., Bao, Z., Jia, F., Deng, S.: Adsorption of CO_2, CH_4, N_2O, and N_2 on MOF-5, MOF-177, and Zeolite 5A. Environ. Sci. Technol. **44**, 1820–1826 (2010)

Sumida, K., Rogow, D.L., Mason, J.A., McDonald, T.M., Bloch, E.D., Herm, Z.R., Bae, T.-H., Long, J.R.: Carbon dioxide capture in metal–organic frameworks. Chem. Rev. **112**, 724–781 (2012)

Tagliabue, M., Farrusseng, D., Valencia, S., Aguado, S., Ravon, U., Rizzo, C., Corma, A., Mirodatos, C.: Natural gas treating by selective adsorption: material science and chemical engineering interplay. Chem. Eng. J. **155**, 553–566 (2009)

Treacy, M.M.J., Higgins, J.B., Higgins, J.B.: Collection of Simulated XRD Powder Patterns for Zeolites. Elsevier B.V, The Netherlands (2001)

Wang, Q., Luo, J., Zhong, Z., Borgna, A.: CO_2 capture by solid adsorbents and their applications: current status and new trends. Energy Environ. Sci. **4**, 42–55 (2011)

Xiao, M., Hu, X., Gong, Y., Gao, D., Zhang, P., Liu, Q., Liu, Y., Wang, M.: Solid transformation synthesis of zeolites from fly ash. RSC Adv. **5**, 100743–100749 (2015)

Yoon, I.S., Kim, S.B.: A study on iron compounds of volcanic basalt at Hantan Riverside in Cheorwon. J. Korean Magn. Soc. **25**, 169–173 (2015)

Yu, K.M.K., Curcic, I., Gabriel, J., Tsang, S.C.E.: Recent advances in CO_2 capture and utilization. Chemsuschem **1**, 893–899 (2008)

Zhao, Y., Nzihou, A., Minh, D.P., Lyczko, N.: A review of biogas utilisation, purification and upgrading technologies. Waste Biomass Valoriz. **8**, 267–283 (2017)

Publisher's Note Springer Nature remains neutral with regard to jurisdictional claims in published maps and institutional affiliations.